DRAL
Daresbury Laboratory
Rutherford Appleton Laboratory

RAL Report
RAL-94-048

Higgs Searches and WW Scattering

R J N Phillips

May 1994

Rutherford Appleton Laboratory Chilton DIDCOT Oxfordshire OX11 0QX

DRAL is part of the Engineering and Physical Sciences Research Council

Rutherford Appleton Laboratory

RAL-94-048
May 1994

HIGGS SEARCHES AND WW SCATTERING

RJN Phillips
Rutherford Appleton Laboratory, Chilton, Didcot,
Oxon, OX11 0QX, England.

Lecture given at WHEPP-3, Third Workshop on High Energy Particle Physics,
at the Institute of Mathematical Sciences, Madras, India, 10-22 January 1994.

1. INTRODUCTION.

This lecture is about aspects of Electroweak Symmetry Breaking (EWSB). There are sections on Higgs searches in the Standard Model (SM), on WW, WZ and ZZ scattering as probes of EWSB, and on Higgs phenomenology in the Minimal Supersymmetric Standard Model (MSSM).

The SM has one complex SU(2)-doublet of scalar fields,

$$\Phi = \begin{pmatrix} \phi^+ \\ \phi^0 \end{pmatrix} = \begin{pmatrix} -iw^+ \\ (-iz + H + v)/\sqrt{2} \end{pmatrix},$$

with vacuum expectation value v arising from the self-interaction

$$V(\Phi) = \lambda[|\Phi|^2 - v^2/2]^2.$$

In the resulting EWSB pattern, where W and Z fields acquire masses, the scalar field components $w^\pm$ and z become the new longitudinal components $W_L^\pm$ and Z_L while H survives as a real SU(2)-singlet scalar field - the Higgs boson - with mass $m_H = \sqrt{2\lambda}v$. To recover standard Fermi couplings we must have $v = (\sqrt{2}G_F)^{-1/2}$, but the quartic coupling λ is not determined *a priori*.

How can we probe the EWSB dynamics?
(i) Look for H^0 ; its mass measures λ; its couplings to W,Z and fermions are prescribed by v and the particle masses, and should be checked.
(ii) Study $W_L^\pm$ and Z_L scattering; they remember their origins as would-be Goldstone bosons $w^\pm$ and z, and their scattering via $V(\Phi)$ will be strong if λ is large.
These strategies, motivated here by the SM case, extend naturally to more general scenarios. We shall mostly illustrate the possibilities for the proposed Large Hadron

Collider LHC at CERN, but for convenience shall also take some examples from studies for the comparable but cancelled SSC project.

2. SM HIGGS SEARCHES AT HADRON COLLIDERS.

Higgs hadroproduction goes mainly through the diagrams in Fig.1 [1]:
(a) $gg \to H$ via heavy quark loops usually gives the biggest rate;
(b) $qq(\bar{q}) \to H$ via WW (or ZZ) fusion is also big, and has taggable jets;
(c) $gg \to t\bar{t}H$ and (d) $q\bar{q}' \to WH$ are smaller but have the advantage that we can tag the leptons from $W \to \ell\nu$ and $t \to bW \to b\ell\nu$.
Fig.2 shows the corresponding lowest-order LHC cross sections, for $m_t = 140$ GeV, and Fig.3 gives the principal decay branching fractions.

2.1 Intermediate mass range.

Light Higgses ($m_H \lesssim M_Z$) should be detectable at LEP1 or LEP2, but the intermediate mass range $M_Z \lesssim m_H \lesssim 2M_Z$ needs higher energy. The dominant $H \to b\bar{b}$ mode was widely believed to be undetectable at hadron colliders, because of enormous $b\bar{b}$ backgrounds from QCD; the $\tau\bar{\tau}$ mode too is interesting but problematical. Until recently, most attention was therefore focussed on the more promising signals from $H \to \gamma\gamma$ and $H \to ZZ^* \to \ell\bar{\ell}\ell'\bar{\ell}'$.

Inclusive $H \to \gamma\gamma$ signals are difficult to see above large backgrounds from $gg, q\bar{q} \to \gamma\gamma$ production and also from $jet + jet$ and $jet + \gamma$ states where $jet \to \pi^0$ fakes γ. To extract a signal requires excellent mass resolution $\delta M_{\gamma\gamma} < 1.5$ GeV and rejection factor $R(jet \to fake\,\gamma) < 10^{-4}$ (see GEM studies for SSC[2]). Fig.4 shows typical predicted $M_{\gamma\gamma}$ distributions, before and after background subtraction. Note the very low signal/background ratios here, requiring very high statistics.

Lepton-tagged $H \to \gamma\gamma$ signals, based on the $t\bar{t}H$ and WH production channels, are smaller but much cleaner since the lepton requirement strongly suppresses backgrounds, so less stringent mass resolution $\delta M_{\gamma\gamma} < 3$ GeV and rejection factor $R(jet \to fake\,\gamma) < 5 \times 10^{-4}$ may suffice (see SDC studies for SSC[3]). Fig.5 shows typical $M_{\gamma\gamma}$ signal and background distributions.

Four-lepton signals, based on $H \to ZZ^*$ decays with one Z off-shell, are also very clean and have a big enough branching fraction for $m_H > 120$ GeV - see Fig.3; the dip near $m_H = 2M_W = 160$ GeV is due to competition from the $H \to W^+W^-$ channel that opens here. After suitable p_T and isolation cuts on the leptons, the backgrounds from continuum ZZ^*, $Zb\bar{b}$, $Zt\bar{t}$ and $t\bar{t}$ production are small; Fig.6 shows typical signal and background curves for an SSC example[3].

Very recently it has been argued that $H \to b\bar{b}$ dijet signals may be detectable after all, with the backgrounds sufficiently suppressed by suitable tagging.
(a) Tag two leptonic W-decays in the $gg \to t\bar{t}H \to (bW^+)(\bar{b}W^-)(b\bar{b})$ channel; this gives a 2-lepton + 4-jet + missing-E_T signature, with a peak at m_H in the dijet invariant mass $m(jj)$ distribution[4]. There is a combinatorial background (from

'wrong' dijet pairings) and a much bigger background from $t\bar{t}jj$ production; a narrow peak from $t\bar{t}Z$ production also has to be calculated and subtracted; but the SSC illustration in Fig.7 suggests this approach could possibly work.
(b) Tag 3 or 4 b-jets in the $gg \to t\bar{t}H \to (bW^+)(\bar{b}W^-)(b\bar{b})$ channel, using a microvertex detector to pick out the displaced vertices from b-decays, and look for a peak in the $2b$ invariant mass spectrum[5]. With sufficiently high b-tag efficiency and purity, all background channels except $t\bar{t}Z$ (with $Z \to b\bar{b}$) and $t\bar{t}b\bar{b}$ are suppressed. Fig.8 shows an SSC illustration with 3-b-tagging; the upper curves assume tagging efficiencies $\epsilon_b = 0.4$ and $\epsilon_g = 0.005$ for b-jets and gluon-jets, respectively; the lower curves (displaced by 100 units) assume values 0.3 and 0.01 instead. Note once more the low signal/background ratios, requiring high statistics in this game ! For LHC, taking $m_H = 100$ GeV and $m_t = 140$ GeV and the less optimistic tagging efficiencies, we need integrated luminosity $L = 200\ fb^{-1}$ to get a signal $S = 600$ events over a background $B = 14000$ events with statistical significance $S/\sqrt{B} = 5$ standard deviations. But the situation improves if t is heavier; with $m_t = 180$ GeV, $L = 60\ fb^{-1}$ is enough to give $S = 210$, $B = 1800$, and $S/\sqrt{B} = 5$ again[5].
(c) Rapidity-gap tagging may also work[6]. The $qq \to qqH$ mechanism has no colour exchange and is therefore unlikely to radiate additional soft gluons or $q\bar{q}$ pairs in the central region, unlike the other H production processes or typical background channels. By requiring that there is no particle production (apart from an $H \to b\bar{b}$ dijet candidate) in a wide central interval of rapidity, it may be possible to suppress backgrounds enough to extract a $qq \to qqH$,$H \to b\bar{b}$ dijet signal. But such rapidity gaps can get filled in by soft interactions of spectator partons ('the underlying event'), or faked by statistical fluctuations. Detailed studies are needed[6]; the intermediate-mass Higgs case has received little attention so far[7].

We see that one or other of the popular $\gamma\gamma$ and 4-lepton signals should be detectable across the whole intermediate mass range $M_Z < m_H < 2M_Z$. New ideas make the $b\bar{b}$ dijet signal appear promising too, at least in the lower part of the range.

2.2 Heavy Higgs searches.

For heavy Higgses ($m_H > 2M_Z$), the decay chain $H \to ZZ \to 4\ell$ offers a very clean 'gold-plated' signal with a nice peak in the invariant mass $m(\ell\ell\ell\ell)$ and relatively little background, mostly from continuum ZZ production. Fig.9 shows cross sections for this signal versus m_H; note that they are an order of magnitude smaller at LHC than at the late lamented SSC, requiring that much more luminosity. Fig.10 shows the mass peaks for $m_H = 600$ and 800 GeV at LHC after suitable cuts[8]. We see that the mass peak broadens and becomes harder to detect as m_H increases; in fact

$$\Gamma_H \simeq (0.5 TeV)(m_H/1\ TeV)^3.$$

Thus the range $m_H < 0.6$ TeV is relatively easy; $m_H > 0.8$ TeV is hard.

An alternative 'silver-plated' $H \to ZZ \to (\ell^+\ell^-)(\nu\bar{\nu})$ signal is also promising. It has a somewhat less clean signature, namely one leptonic Z plus missing-E_T, but

has six times bigger branching fraction than the gold-plated signal - which could be helpful at large m_H . The main backgrounds from $Z + jets$, $t\bar{t}$ and ZZ continuum production can be suppressed by suitable cuts, especially by requiring large missing-E_T, since the $H \to ZZ$ decay gives a Jacobian peak near $p_T(Z) = \frac{1}{2}\sqrt{m_H^2 - 4M_Z^2}$ that translates into a peak in missing-E_T; see Fig.11. The mass m_H can be estimated from the missing-E_T distribution, but a cleaner estimate (from a narrower peak) can be made using the 'transverse mass' variable $m_T(\ell\ell, \nu\nu)$[9] defined by

$$m_T(\ell\ell, \nu\nu)^2 = [\sqrt{p_T(\ell\ell)^2 + M_Z^2} + \sqrt{p_T(\nu\nu)^2 + M_Z^2}]^2 - [\vec{p_T}(\ell\ell) + \vec{p_T}(\nu\nu)]^2$$

where $\vec{p_T}(\nu\nu) = \vec{E_T}$-missing. Both $p_T(\ell\ell)$ and $p_T(\nu\nu)$ have Jacobian peaks that are smeared by the transverse motion of H, but this smearing approximately cancels in the combination m_T.

The $H \to W^+W^- \to (\ell\nu)(\ell'\nu')$ signal has the biggest branching fraction of the all-leptonic modes; the signature is two isolated large-p_T leptons plus missing-E_T, but there is a horrendous background from $t\bar{t} \to bW^+\bar{b}W^-$. A strategy of jet-tagging and anti-tagging (vetoing) has been proposed to rescue this signal. Note first that the important $qq \to qqH$ production subprocess (see Figs.1 and 2) contains two jets with typically large pseudo-rapidity $|\eta| \sim 3 - 5$, but no central jets when $H \to \ell\nu\ell'\nu'$. In contrast, the QCD background process $gg, q\bar{q} \to t\bar{t} \to bW^+\bar{b}W^-$ contains typically no forward jets but has two central b-jets. Hence, by requiring at least one forward jet with $3 < |\eta| < 5$ and no central jet with $|\eta| < 3$, the background can be suppressed relative to the signal. [Jet tagging/vetoing can help to reduce backgrounds to the previous $H \to ZZ$ signals also]. It has been shown that the $H \to WW$ signal can be separated by these and other suitable cuts, at least for $0.6 \lesssim m_H \lesssim 1$ TeV[10]. The mass m_H can then be estimated from the dilepton invariant mass $m(\ell\ell')$ or another transverse mass $m(\ell\ell', \nu\nu')$ defined by[11]

$$m_T(\ell\ell', \nu\nu')^2 = [\sqrt{p_T(\ell\ell')^2 + m(\ell\ell')^2} + p_T(\nu\nu')]^2 - [\vec{p_T}(\ell\ell') + \vec{p_T}(\nu\nu')]^2$$

where $\vec{p_T}(\nu\nu') = \vec{E_T}$-missing; this differs from the previous transverse mass variable because we no longer have the constraints $m(\ell\ell) = m(\nu\nu) = M_Z$ and indeed $m(\nu\nu')$ cannot be measured. These variables peak at $m(\ell\ell') \simeq \frac{1}{2}m_H$ and $m_T(\ell\ell', \nu\nu') \simeq \frac{3}{4}m_H$, respectively.

Combining the coverage of $H \to ZZ \to 4\ell$, $H \to ZZ \to 2\ell 2\nu$ and $H \to WW \to 2\ell 2\nu$ signals, we see that heavy Higgses will be detectable for $m_H \lesssim 1$ TeV.

2.3. Studying Higgs couplings separately.

In principle, the strengths of H couplings to WW, ZZ, tt, $b\bar{b}$ can be separated in various ways; examples follow. Note that the signal rate in each particular channel has the general form

$$\sigma(pp \to H \to channel) = \sigma(pp \to H) \times \Gamma(H \to channel)/\Gamma_H$$

(a) The dominant untagged or lepton-tagged $\gamma\gamma$ signals depend directly on the $Ht\bar{t}$ coupling, both at the H production vertex (t-quark loop or associated production with $t\bar{t}$) and at the H decay (via t-quark loop), but the total decay width in the denominator is dominated by $Hb\bar{b}$ at the relevant low-intermediate masses. Thus the rate determines $(Ht\bar{t})^4/(Hb\bar{b})^2$ approximately.
(b) If the WH and $t\bar{t}H$ lepton-tagged $\gamma\gamma$ signals can be separated via final-state criteria, their ratio will determine

$$(WH \to \gamma\gamma\ rate)/(t\bar{t}H \to \gamma\gamma\ rate) \sim (HWW)^2/(Ht\bar{t})^2$$

(c) The $t\bar{t}H \to t\bar{t}(b\bar{b})$ tagged dijet signals depend on the $Ht\bar{t}$ coupling for H production, with branching fraction $B(H \to b\bar{b}) \sim 1$ for decay. Thus the signal rate determines $(Ht\bar{t})^2$ approximately, and the ratio to $\gamma\gamma$ rates determines

$$(tagged\ bb\ dijet\ rate)/(\gamma\gamma\ rate) \sim (Hb\bar{b})^2/(Ht\bar{t})^2.$$

(d) For high-intermediate masses $m_H > 120$ GeV, the total width Γ_H depends non-trivially on $Hb\bar{b}$, HWW and HZZ couplings, so nothing simple can be said about the $H \to 4\ell$ signals here
(e) For heavy Higgses, the ratio of WW/ZZ signals could determine the ratio of $(HWW)/(HZZ)$ couplings.
(f) The ratio of jet-tagged/untagged heavy Higgs signals could determine the ratio of $qq \to qqH$ and $gg \to H$ production mechanisms, that depends directly on the $(HVV)/(Ht\bar{t})$ coupling ratio, where $V = W, Z$ but W dominates.
(g) Γ_H for a heavy Higgs, directly measurable from the width of the mass peak, should be dominated by the HWW coupling with smaller contributions from HZZ and $Ht\bar{t}$.

3. WW, WZ AND ZZ SCATTERING.

In the SM, the coupling strength of the scalar potential is

$$\lambda = \frac{m_H^2}{2v^2} = [\frac{m_H}{348GeV}]^2$$

which is large if H is heavy, implying strong scattering of the Goldstone bosons $w^{\pm}$ and z that become $W_L^{\pm}$ and Z_L. This can also happen more generally, outside the SM. Figure 12 shows a generic W_L, Z_L scattering process at LHC. Different final states are sensitive to different physics: $W_L^+W_L^-$ and Z_LZ_L states probe Higgs-like resonances; $W_L^+W_L^+$ and $W_L^-W_L^-$ states probe non-resonant scattering (except in some exotic models); W_LZ_L states probe techni-ρ-type resonances.

The idea is that enhanced WW, WZ, ZZ production may be attributed to strong W_L and Z_L scattering, since the transversely polarized states W_T and Z_T only have the weak $SU(2) \times U(1)$ gauge interactions. Details of the enhancement will shed light on EWSB. To discuss this scattering, we must first introduce a number of ideas, approximations and constraints.

3.1 The effective W approximation (EWA).

In analogy with the Weizsäcker-Williams approximation for photons, the incident quark beams can be replaced by beams of approximately on-shell W and Z bosons. Writing $P^{\alpha}_{W/q}(x)$ as the known probability distribution (splitting function) for finding a W with polarization α and momentum fraction x in quark q, the subprocess cross section for $q_1 q_2 \to q_3 q_4 W_3^{\gamma} W_4^{\delta}$ is

$$\sigma(q_1 q_2 \to q_3 q_4 W_3^{\gamma} W_4^{\delta}) = \sum_{\alpha,\beta} \int dx_1 dx_2 P^{\alpha}_{W1/q1}(x_1) P^{\beta}_{W2/q2}(x_2) \sigma(W_1^{\alpha} W_2^{\beta} \to W_3^{\gamma} W_4^{\delta})$$

The physical cross section for $pp \to q_3 q_4 W_3 W_4 X$ is found by further integrating over incident quark distributions and summing over final W spins. The splitting functions for W_L and Z_L are

$$P^L_{W^+/u} = P^L_{W^-/d} = P^L_{W^+/\bar{d}} = P^L_{W^-/\bar{u}} = \frac{g^2}{16\pi^2} \frac{(1-x)}{x},$$

$$P^L_{Z/q} = P^L_{Z/\bar{q}} = \frac{g^2}{32\pi^2} \frac{1 - 4x_W|Q| + 8x_W^2 Q^2}{1 - x_W} \frac{(1-x)}{x},$$

where $x_W = \sin^2\theta_W = 0.23$, Q is the electric charge of quark q and $g^2 = 8M_W^2 G_F/\sqrt{2}$ is the SU(2) gauge coupling squared. The EWA is the only known way to separate the contributions of W_L and Z_L scattering in a high energy process. The approximation is collinear and neglects transverse momenta for the initial W_1, W_2 and for the recoiling quarks q_3, q_4.

3.2 The Goldstone Boson Equivalence Theorem (GBET).

This theorem[12] relates any scattering amplitude for real W_L and Z_L to the amplitude for the corresponding Goldstone bosons w and z:

$$M[W_L(p_1), W_L(p_2), ...] = M[w(p_1), w(p_2), ...]_R + \mathcal{O}(M_W/E_W),$$

where R indicates a renormalizable R_ξ gauge. The p_i are momenta (masses are neglected here). The EWA provides essentially real incoming W_L and Z_L; the GBET allows us to compute their scattering from any given model of the Goldstone boson sector, up to corrections of order M_W/E_W.

3.3 Isospin, crossing and unitarity.

The various ww, wz and zz scattering amplitudes are all related by SU(2) isospin and crossing symmetries, just like $\pi\pi$ scattering. In terms of components w_i ($i = 1,2,3$; $w^{\pm} = (w_1 \mp w_2)/\sqrt{2}$, $z = w_3$), the general amplitude has the form

$$M(w_a w_b \to w_c w_d) = A(s,t,u)\delta_{ab}\delta_{cd} + A(t,s,u)\delta_{ac}\delta_{bd} + A(u,t,s)\delta_{ad}\delta_{bc},$$

where $s = (p_a + p_b)^2$, $t = (p_a - p_c)^2$, $u = (p_a - p_d)^2$ and A is symmetrical in its last two arguments: $A(s,t,u) = A(s,u,t)$. In terms of this single basic amplitude A, the various channel amplitudes are

$$\begin{aligned} M(w^+w^- \to w^+w^-) &= A(s,t,u) + A(t,s,u), \\ M(w^+w^- \to zz) &= A(s,t,u), \\ M(zz \to zz) &= A(s,t,u) + A(t,s,u) + A(u,t,s), \\ M(w^\pm z \to w^\pm z) &= A(t,s,u), \\ M(w^+w^+ \to w^+w^+) &= A(t,s,u) + A(u,t,s). \end{aligned}$$

The amplitudes for s-channel isospin $T = 0, 1, 2$ are

$$\begin{aligned} M(T=0) &= 3A(s,t,u) + A(t,s,u) + A(u,t,s), \\ M(T=1) &= A(t,s,u) - A(u,t,s), \\ M(T=2) &= A(t,s,u) + A(u,t,s). \end{aligned}$$

These pure-isospin channels diagonalize the S-matrix, so their s-channel partial wave amplitudes a_L^T defined by

$$M(T) = 32\pi \sum_L (2L+1)\, a_L^T\, P_L(\cos\theta)$$

should satisfy the unitarity condition $|2a_L^T - i| \leq 1$, i.e. lie within a circle in the complex plane.

3.4 Low energy theorem (LET).

In the low-energy limit, Goldstone boson scattering is expected to be controlled by the dynamics of EWSB. Since EWSB in the SM is essentially the non-linear sigma model with chiral $SU(2) \times SU(2)$ symmetry, it has been pointed out[13] that the low-energy theorems of $\pi\pi$ scattering[14] can be directly applied to the case of w and z scattering, simply replacing the pion decay constant $F_\pi = 94$ MeV by the vev $v = 246$ GeV. Hence in all channels the threshold behaviour is approximately specified by v:

$$A(s,t,u) \simeq s/v^2.$$

Hence the low-energy partial wave amplitudes are

$$a_0^0 = \frac{s}{16\pi v^2},\ a_1^1 = \frac{s}{96\pi v^2},\ a_0^2 = -\frac{s}{32\pi v^2}.$$

This linear rise with s cannot be extrapolated indefinitely without violating unitarity. Strictly speaking, since these formulae give purely real a_L^T, any non-zero value lies outside the unitarity circle, but this could at first be cured by adding a small imaginary part. However, the real part of a_0^0 exceeds its unitarity limit $\Re a_L^T \leq \frac{1}{2}$ when $\sqrt{s} >$

$\sqrt{8\pi}v = 1.2$ TeV, while the T=2 amplitude exceeds this limit for $\sqrt{s} > 1.7$ TeV. We see that unitarity is likely to be an important constraint in the TeV range.

3.5 Models for Goldstone boson scattering.

A wide variety of models have been proposed, to illustrate and parameterize the scattering of $w^{\pm}$ and z. We confine ourselves here to the models evaluated in a recent survey by Bagger et al[15] of possible strong WW, WZ, ZZ scattering at hadron colliders.

(i) Standard Model.
This gives the form

$$A(s,t,u) = \frac{-m_H^2}{v^2}(1 + \frac{m_H^2}{s - m_H^2 + im_H\Gamma_H\theta(s)}),$$

where m_H is the Higgs mass, $v = 246$ GeV is the usual vev, and a Breit-Wigner form has been imposed for the Higgs resonance. θ is the step-function: $\theta(s) = 1(0)$ for $s > 0(s \leq 0)$. $A(t,s,u)$ and $A(u,t,s)$ are obtained by permuting s,t,u. For illustration we shall take $m_H = 1$ TeV[15].

(ii) O(2N) Model [16].
Motivated by the isomorphism between $SU(2)_L \times SU(2)_R$ and $O(4)$ symmetries, and using a large-N approximation, this model gives

$$A(s,t,u) = \frac{16\pi^2 s}{16\pi^2 v^2 - sN[2 + \ln(\Lambda^2/|s|) + i\pi\theta(s)]},$$

where $\theta(s)$ is the step-function as before. Following Ref.[15], we take the case $N = 2$ with physical cut-off $\Lambda = 3$ TeV.

(iii) Chirally-Coupled Scalar Model[15].
This model describes the low-energy behaviour of a technicolor-type model with a techni-sigma scalar resonance, through the amplitude

$$A(s,t,u) = \frac{s}{v^2} - (\frac{g^2 s^2}{v^2})\frac{1}{s - M_S^2 + iM_S\Gamma_S\theta(s)},$$

where M_S and Γ_S are the scalar resonance mass and its decay width into Goldstone fields, $\Gamma_S = 3g^2 M_S^3/(32\pi v^2)$. We choose $M_S = 1.0$ TeV and $\Gamma_S = 0.35$ TeV, following Ref.[15].

(iv) Chirally-Coupled Vector Model[15, 17].
This model describes the low-energy behaviour of a technicolor-type model with a techni-rho vector resonance, through the amplitude

$$A(s,t,u) = \frac{s}{4v^2}(4 - 3a) + \frac{aM_V^2}{4v^2}[\frac{u - s}{t - M_V^2 + iM_V\Gamma_V\theta(t)} + \frac{t - s}{u - M_V^2 + iM_V\Gamma_V\theta(u)}],$$

where M_V and Γ_V are the vector resonance mass and width while $a = 192\pi v^2\Gamma_V/M_V^3$. We choose the two cases $M_V = 2.0$ TeV with $\Gamma_V = 0.7$ TeV and $M_V = 2.5$ TeV with $\Gamma_V = 1.3$ TeV, following Ref.[15].

(v) LET-CG Model[13]
This model simply extrapolates the low-energy amplitudes, prescribed by low-energy theorems (LET) in terms of the vev v:

$$A(s,t,u) = s/v^2.$$

These amplitudes eventually violate unitarity, as we saw above, so the partial wave amplitudes are held constant after they reach the bound $|a_L^T| \leq 1$ (less stringent than the bound $\Re a_L^T \leq \frac{1}{2}$ we mentioned earlier).

(vi) LET-K Model[18].
Here the LET amplitudes above are unitarized instead by the K-matrix prescription,

$$a_L^T \to a_L^T/(1 - ia_L^T),$$

that enforces the elastic unitarity condition $|2a_L^T - i| = 1$.

(vii) Delay-K Model[15].
This is an example of non-resonant models, based on an effective Lagrangian method[19]. To order p^4 in the momentum expansion, all model amplitudes have the form

$$A(s,t,u) = \frac{s}{v^2} + \frac{1}{4\pi^2 v^4}(2L_1(\mu)s^2 + L_2(\mu)(t^2+u^2))$$
$$+\frac{1}{16\pi^2 v^4}[-\frac{t}{6}(s+2t)\ln(\frac{-t}{\mu^2}) - \frac{u}{6}(s+2u)\ln(\frac{-u}{\mu^2}) - \frac{s^2}{2}\ln(\frac{-s}{\mu^2})],$$

where μ is the renormalization scale and $L_i(\mu)$ are renormalized coefficients in the effective Lagrangian. The parameters $L_1(\mu)$, $L_2(\mu)$ and μ essentially cover all possible non-resonant physics in this approximation. Following Ref.[15] we choose the example $L_1(\mu) = -0.26$, $L_2(\mu) = 0.23$ with $\mu = 1.5$ TeV, for which unitarity breakdown is delayed until $\sqrt{s} = 2$ TeV. These amplitudes are complex; for simplicity, unitarity is imposed by the K-matrix prescription based on the real part of a_L^I, i.e. $a_L^I \to \Re a_L^I/(1 - i\Re a_L^I)$.

3.6 Model results

At a hadron collider we can only hope to recognize $W \to \ell\nu$ and $Z \to \ell\ell$ leptonic final states in the face of QCD multijet backgrounds. Even so, there remain backgrounds from electroweak W and Z production, from Drell-Yan lepton pairs and from the semileptonic decays of heavy quarks. Selection cuts to enhance signal/background include lepton isolation, high lepton p_T, central leptons with $|\eta(\ell)| \lesssim 2$, high invariant mass $m(\ell\ell')$ for WW and $m(ZZ)$ for ZZ ; in WW cases it also helps to require the two leptons to be back-to-back in azimuth and have high relative momentum.

Finally, it can be helpful to tag one of the spectator jets and/or veto central jets with $|\eta(j)| < 3$ (as in Section 2.2 for heavy Higgs searches). The following table shows results from Ref.[15] for the LHC, with typical realistic cuts. The signals here are the total production of $W_L W_L \to \ell\nu\ell\nu$ (etc); the background column (Bkgd) includes SM production of $W_T W_T$, $W_T W_L$ (etc) calculated using small m_H.

Events for luminosity $100 fb^{-1}$, assuming $m_t = 140$ GeV, $\sqrt{s} = 16$ TeV.

Case	*Bkgd*	*SM*	*Scalar*	*O(2N)*	*Vec2.0*	*Vec2.5*	*LETCG*	*LETK*	*DelayK*
ZZ	0.1	3.9	2.7	1.8	0.4	0.6	1.1	0.9	0.6
W^+W^-	15	32	21	16	7.4	6.1	8.3	6.3	5.5
W^+Z	0.3	0.3	0.4	0.3	3.3	1.8	1.6	1.4	1.7
W^+W^+	1.7	3.7	5.2	4.3	4.8	7.3	16	14	8.3

We see that every model predicts a signal in at least one channel, although more luminosity would be desirable, and that the different channels are helpfully complementary. There seem to be good prospects for probing EWSB via weak boson scattering.

Fig.13 illustrates some of the more promising signals versus invariant mass $m(ZZ)$ for ZZ, $m(\ell\ell')$ for WW and a suitable $\ell\ell\ell\nu$ transverse mass variable m_T for WZ cases [15]. These illustrations are for the defunct SSC, but something similar should hold for LHC.

4. SUSY HIGGS POSSIBILITIES AT LEP AND LHC.

The Higgs sector is the shakiest part of the SM, where something extra may well be added. Let us consider the new degrees of freedom coming from some possible extensions[1].
(a) SM has one complex scalar doublet ϕ with vev $\sqrt{2} < \phi^0 > = v = 246$ GeV. Its 4 degrees of freedom show up as W_L^+, W_L^-, Z_L and H^0. There is just 1 free parameter m_H in the scalar sector.
(b) MSSM (minimal SUSY SM) has two scalar doublets with $\sqrt{2} < \phi_1^0 >= v \cos\beta$ and $\sqrt{2} < \phi_2^0 >= v \sin\beta$. Their 8 degrees of freedom show up as W_L^+, W_L^-, Z_L plus five spin-0 Higgs bosons h^0, H^0, A^0, H^+, H^-. h^0 and H^0 have $CP = +1$ (by convention $m_h < m_H$) and A has $CP = -1$. There are now 2 free parameters, often taken to be m_A and $\tan\beta = v_2/v_1$.
(c) NMSSM (next-to-minimal SUSY SM) has an extra neutral singlet scalar field n with vev $< n > = x$ non-zero but free. The 10 degrees of freedom show up as W_L^+, W_L^-, Z_L plus seven spin-0 Higgs bosons h^0, H_1^0, H_2^0, A_1^0, A_2^0, H^+ , H^- (where A_1 and A_2 have $CP = -1$). The number of free parameters now jumps to 6, however, because there are suddenly many more possible terms in the general scalar potential. This model has a richer spectrum and also looser limits.
For today we shall concentrate on the more constrained example of MSSM.

4.1 MSSM at tree level.

All MSSM Higgs masses and couplings, plus a mixing angle α that relates h and H to $\Re\phi_1$ and $\Re\phi_2$, are determined at tree level by m_A and $\tan\beta$:

$$\begin{aligned} \tan 2\alpha &= \tan 2\beta\,(m_A^2 + M_Z^2)/(m_A^2 - M_Z^2) \\ m_h^2, m_H^2 &= \frac{1}{2}[m_A^2 + M_Z^2 \mp \sqrt{(m_A^2 + M_Z^2)^2 - 4m_A^2 M_Z^2 \cos^2 2\beta}] \\ m_{H\pm}^2 &= m_A^2 + M_W^2 \end{aligned}$$

with $-\frac{\pi}{2} \leq \alpha \leq 0$. Hence at tree level

$$m_h \leq M_Z, m_A \; ; \; m_H \geq M_Z \; ; \; m_{H\pm} \geq M_W, m_A.$$

Thus there is always at least one Higgs boson h lighter than Z. However, in the limit $m_A \gg m_Z$, all the other bosons H, A and $H^\pm$ become very heavy and approximately degenerate while $m_h \simeq M_Z \cos 2\beta$, so it is conceivable that only this one light boson may be accessible.

4.2 MSSM with radiative corrections.

MSSM Higgs physics does not depend only on the scalar-sector parameters m_A and $\tan\beta$, but also has important loop corrections because the top quark is so heavy (Fig.14). These radiative corrections depend on m_t, $m_{\tilde{t}}$ (the mean t-squark mass), m_Q, m_U and m_D (soft SUSY-breaking squark masses), A_t and A_b (coefficients of trilinear $\tilde{t}_L\tilde{t}_R\phi_2$ and $\tilde{b}_L\tilde{b}_R\phi_1$ soft SUSY-breaking terms), and μ (coefficient of $\phi_1\phi_2$ mixing in the superpotential); see e.g. Ref.[20]. This dependence is mainly on m_t and (logarithmically) on $m_{\tilde{t}}$; neglecting the other parameters, the upper limit on m_h becomes

$$m_h^2 \leq M_Z^2 + \frac{3g^2 m_t^4}{4\pi^2 M_W^2} \ln(m_{\tilde{t}}/m_t),$$

in one-loop approximation.

In the following we shall estimate these radiative corrections by assuming that $m_t \simeq 150$ GeV, $m_{\tilde{t}} \simeq 1$ TeV, and that squark mixing is moderate (explicitly $m_Q = m_U = m_D = 2A_t = 2A_b = 4\mu = 1$ TeV, following Ref.[21]). With this choice, the m_h upper limit is $m_h \lesssim 115$ GeV; the full dependence of m_h, m_H and $m_{H\pm}$ on the remaining parameters m_A and $\tan\beta$ is shown in Fig.15[21]. Searches for h at LEP1 (via $e^+e^- \to Zh, Ah$) have already covered the region $m_h \lesssim 50$ GeV, depending somewhat on $\tan\beta$; the higher energy $\sqrt{s} \sim 170 - 190$ GeV at LEP2 will arguably allow searches up to $m_h \sim 90$ GeV; but Fig.15 shows there is a large region of parameter space ($m_A \gtrsim 90$ GeV, $\tan\beta \gtrsim 2$) where h and all the heavier Higgses could be hiding undetected. This is LHC territory.

Compared to the SM Higgs coupling to fermions and gauge bosons, given by $L = -(m_i/v)\bar{f}_i f_i H + \frac{1}{2}g^2 vWWH + \frac{1}{4}(g^2 + g'^2)vZZH$, the MSSM neutral Higgs couplings

have the following extra factors:

	h	H	A
$t\bar{t}$	$\cos\alpha/\sin\beta$	$\sin\alpha/\sin\beta$	$-i\gamma_5\cot\beta$
$b\bar{b},\ \tau\bar{\tau}$	$-\sin\alpha/\cos\beta$	$\cos\alpha/\cos\beta$	$-i\gamma_5\tan\beta$
$WW,\ ZZ$	$\sin(\beta-\alpha)$	$\cos(\beta-\alpha)$	
ZA	$\cos(\beta-\alpha)$	$\sin(\beta-\alpha)$	

We see that h and H share their coupling strengths, that A does not couple directly to WW, ZZ or ZA, and that for large $\tan\beta$ (small $\cos\beta$) all the $b\bar{b}$ couplings are greatly enhanced. These coupling factors vary enormously as α varies, across the $(m_A, \tan\beta)$ plane.

The charged scalars $H^\pm$ couple to typical fermions by

$$L = \frac{g}{2\sqrt{2}M_W} H^+ [m_t V_{tb}\cot\beta\ \bar{t}(1-\gamma_5)b + m_b V_{tb}\tan\beta\ \bar{t}(1+\gamma_5)b$$
$$+ m_c V_{cs}\cot\beta\ \bar{c}(1-\gamma_5)s + m_\tau\tan\beta\ \bar{\nu}(1+\gamma_5)\tau],$$

but have no tree-level coupling to WZ.

These new coupling factors and new kinds of coupling show that the production and decay of MSSM Higgses are not just trivial extensions of the SM situation, in general. There is however one particularly simple region, where m_A becomes large ($\gtrsim 300$ GeV); here A, H and $H^\pm$ become approximately degenerate, α approaches $\beta - \pi/2$, and all h couplings approach SM values. In this region, h fakes H_{SM} while the heavier Higgses are largely irrelevant; we essentially recover the SM but with the extra constraint $m_h \lesssim 130$ GeV (from MSSM with radiative corrections), whereas the SM alone has a much weaker bound $m_{HSM} \lesssim 600 - 1000$ GeV from triviality and perturbative-unitarity considerations.

4.3 Parameter constraints.

What are the constraints on the MSSM parameters $\tan\beta$ and m_A ?
(a) Requiring the charged-Higgs couplings to $t\bar{b}$ above to remain perturbative gives $m_t/500GeV \lesssim \tan\beta \lesssim 500GeV/m_b$ [22]; the precise limits are somewhat subjective. Essentially, values $\tan\beta << 1$ and $\tan\beta >> 30$ are disfavoured.
(b) Proton decay sets limits in SUSY-GUT models, typically $\tan\beta \lesssim 85$ [23].
(c) Since up-type (down-type) quarks get their masses via the vev v_2 (v_1), the empirical mass hierarchy $m_c >> m_s$ and $m_t >> m_b$ suggests a corresponding hierarchy of vevs $v_2 >> v_1$, i.e. $\tan\beta >> 1$[24].
(d) SUSY-GUT models generally find solutions with $1 \lesssim \tan\beta \lesssim m_t/m_b$. For example, Ref.[25] obtains solutions with $2 < \tan\beta < 40$ while Ref.[26] finds solutions in the range $0.6 < \tan\beta < 60$.
(e) SUSY-GUT models where electroweak symmetry is broken radiatively (a Higgs mass-square goes negative during evolution downward from the GUT scale) require

$\tan\beta > 1$ (see e.g. Ref.[25]).
The consensus on $\tan\beta$ is therefore

$$0 \lesssim \tan\beta \lesssim 60.$$

What now about the other parameter, m_A ?
(f) Higgs boson searches at LEP1 give $20\ GeV \lesssim m_A$ (assuming $\tan\beta > 1$).
(g) In SUSY-GUT models, $m_A \lesssim M_{SUSY} \lesssim 1 - 2$ TeV.
(h) Global electroweak analysis in the MSSM finds a preferred value for m_A below 100 GeV or so, but much larger values are not excluded [27].
The consensus on m_A is therefore

$$20\ GeV \lesssim m_A \lesssim 1 - 2\ TeV.$$

Various other indirect constraints should also be mentioned.
(i) LEP1 searches for $e^+e^- \to H^+H^-$ exclude a parameter region with $\tan\beta < 0$ [28].
(j) Virtual $H^\pm$ can contribute to $B \to \tau\nu X$, but essentially not to $B \to e\nu X$, $\mu\nu X$, breaking lepton universality. The ALEPH measurement of $B(B \to \tau\nu X)$ sets a limit on this contribution and hence a bound $\tan\beta < 0.54(m_H/1\,GeV)$ [29]. This is not very stringent, because the virtual $H^\pm$ and standard $W^\pm$ contributions add incoherently, i.e. a 10% amplitude gives only a 1% correction.
(k) Virtual H^-t loop contributions to $b \to s\gamma$ decays apparently offer a much more stringent constraint; they add coherently to the SM W^-t loop amplitudes. Neglecting possible additional SUSY loops, the present CLEO upper bound on $B(B \to \gamma X) \simeq B(b \to s\gamma)$ gives rather strong lower bounds on the charged-Higgs mass and hence on regions of the $(m_A, \tan\beta)$ plane [30]. However, in the present MSSM context we cannot ignore SUSY loops, especially chargino-stop loops, that can interfere strongly and destructively with the SM amplitude[31]. To apply this constraint we need more information about the sparticle spectrum, e.g. a complete SUSY-GUT model with all masses and mixings prescribed.

4.4 MSSM Higgs production and decay at LHC.

Production and decay of neutral Higgses can proceed by the SM processes, modulo the additional factors discussed above. However, there are new non-SM decay modes like $h \to AA$, $H \to AZ$, $H \to hh$, that tend to dominate when kinematically allowed, blotting out the familiar SM signals in various regions of parameter space; see Fig.16. Note that $H \to hh$ is allowed almost everywhere (except in the shaded region and along a dashed line where the Hhh coupling vanishes), making H usually hard to detect at LHC.

Production of charged Higgses is copious only via top production with $t \to bH^+$ decays, when $m_{H^\pm} < m_t - m_b$; in this case the principal decays are $H^\pm \to cs, \tau\nu$ and the signal could be excess taus compared to other leptons [32]. But for heavier $m_{H^\pm} > m_t$ there can still be signals from $gg \to t\bar{b}H^-$ production with $H^- \to b\bar{t}$ decay, leading to a $bb\bar{b}\bar{b}W^+W^-$ final state; multiple b-tagging is essential here[33].

There are regions of SUSY parameter space where SUSY decay modes like $h \to \chi_1^0\chi_1^0$ to lightest neutralino pairs are allowed; this is potentially dangerous since χ_1^0 is usually the lightest sparticle (LSP), stable, weakly interacting and essentially invisible. However, after LEP1 constraints there remains only a very small parameter range where this decay dominates; unless we are very unlucky, this may dilute the standard signals a bit but will not wash them out. Other decays like $A \to \chi_2^0\chi_2^0 \to (\ell^+\ell^-\chi_1^0)(\ell^+\ell^-\chi_1^0)$ might provide interesting new signals[34].

4.5 Expected MSSM Higgs signals.

For neutral Higgses, the strategy has been first to think about SM-like signals in conventional $\gamma\gamma$ and 4-lepton channels, and also in $b\bar{b}$ and $\tau\bar{\tau}$ channels; h, H and A can all in principle give such signals. For charged Higgses, the emphasis has been mostly on $t \to bH^+ \to b\tau\nu$ signals.

Four groups have made extensive calculations for LHC and SSC, covering the range $m_A > 20$ GeV and $0 < \tan\beta < 50$ [21, 35, 36, 37]. All get broadly similar results, including radiative corrections but mostly ignoring possible SUSY decay modes, and estimate in what regions of parameter space the various MSSM Higgs signals would be detectable. Typical results from Ref.[21] for $m_t = 150$ GeV are shown in Fig.17. Notice that H and A have only small detectability regions for these standard signals, and even the h regions are restricted, although the MSSM $\to$ SM limiting region ($m_A \to$ large) is covered as we would expect. In fact, the conventional $h, H, A \to \gamma\gamma$, ZZ^*, ZZ and $t \to H^+b$ searches do not cover the whole $(m_A, \tan\beta)$ parameter plane. Even when we include LEP1 and LEP2 search potential, there is an intermediate region, approximately $110 < m_A < 160$ GeV and $\tan\beta > 3$ (depending on your choice of m_t and authors), where none of the usual signals would be detectable.

There have been various responses to this inaccessible area (IA).
(a) Additional signals from $H \to \tau\tau$ and $A \to \tau\tau$ could possibly cover the large-$\tan\beta$ part of the IA[37], but identifying and measuring tau pairs is very difficult.
(b) Additional signals from $A \to Zh \to \ell\ell\tau\tau$ would not reduce the IA; neither would new $A \to \chi_2^0\chi_2^0 \to \ell\ell\ell\ell$+missing-$p_T$ signals[34].
(c) SUSY-GUT models have attractive solutions where the top Yukawa coupling λ_t approaches a fixed point (see e.g. Ref.[26]) and gives a constraint $m_t \simeq (200\ GeV)\ \sin\beta$. With $m_t \simeq 150 - 170$ GeV, this defines a small-$\tan\beta$ region outside the IA, and incidentally predicts that h is light enough to be discovered at LEP2 [38]. However, even in this optimistic scenario, not all 5 Higgses can be simultaneously detectable.
(d) With efficient multiple-b-tagging, the signals from $t\bar{t}h(H,A) \to bbbbWW$ or $b\bar{b}h(H,A) \to bbbb$ could be visible at LHC. For $\tan\beta \gtrsim 5$, where the Higgs couplings to b are enhanced, Ref.[39] argues that it will be possible to detect either A and h, or A and H, and essentially remove the IA. Fig.18 shows discovery regions at the two-sigma level for luminosity 100 fb^{-1} = one LHC year (i.e. the two-sigma level after four years) with $m_t = 150$ GeV and $m_{\tilde{t}} = 1$ TeV; the boundary curves marked

h, i, j, k, l, m correspond to ttH, tth, ttA, bbH, bbh, bbA signals respectively, and the label lies on the detectable side[39].
(e) Alternatively, e^+e^- colliders with energy above LEP2 (where $\sqrt{s} \simeq 170 - 190$ GeV at most is planned) would be able to find at least one of the neutral Higgses via $e^+e^- \to hZ, hA, HZ, HA$ searches, since there is an upper bound on m_h. Fig.19 shows the necessary conditions on $\sqrt{s}$ and luminosity $\mathcal{L}$ to cover the whole $(m_A, \tan\beta)$ half-plane with $\tan\beta > 1$, using $Zh \to \tau\tau jj, \ell\ell jj, \nu\nu jj$ and $jjjj$ final states with b-tagging [40]. The condition depends on m_t because of radiative corrections ($m_{\tilde{t}} = 1$ TeV is assumed here).

4.6 Summary.

(a) The five MSSM Higgses have a richer spectrum than the SM, but are in some ways more elusive.
(b) The lightest scalar mass is bounded much more stringently than in the SM.
(c) There will be evidence for physics beyond the SM if we find any neutral scalar with non-SM coupling, or more than one neutral scalar, or a charged scalar.
(d) The principal Higgs-sector parameters are m_A and $\tan\beta$, with radiative corrections controlled mostly by m_t and $m_{\tilde{t}}$. Masses, couplings, production and decay – and hence Higgs signals – vary strongly across the $(m_A, \tan\beta)$ plane.
(e) LEP1 plus LEP2 coverage in this plane is limited (approximately to the $m_h < 90$ GeV region in Fig.15(a).
(f) LHC coverage (earlier SSC studies are similar) of the remaining parameter space was thought to be incomplete; but recent studies of $tth(H, A) \to bbbbWW$ and $bbh(H, A) \to bbbb$ signals assuming efficient multiple-b-tagging remove this weakness.
(g) An e^+e^- collider with energy just a little way above LEP200 could also guarantee to see at least h.
(h) Future useful signals could include $A \to Zh \to \ell\ell\tau\tau$, $A \to \chi_2^0\chi_2^0 \to 4\ell$+missing-$p_T$, heavy $H^\pm \to tb$.
(i) Future theory constraints could come from SUSY-GUT refinements and $b \to s\gamma$.

References

1. For a review of Higgs phenomenology, see J.F. Gunion, H.E. Haber, G.L. Kane, S. Dawson, "The Higgs- Hunter's Guide", Addison- Wesley (1990).
2. GEM collaboration: Letter of Intent GEM TN-92-49 (Nov.1991).
3. SDC collaboration: Technical Design Report SDC-92-201 (April 1992).
4. T. Garavaglia, W. Kwong, D.-D. Wu, Phys. Rev. **48**, R1899 (1993).
5. J. Dai, J.F. Gunion, R. Vega, Phys. Rev. Lett. **71**, 2699 (1993).
6. Y.L. Dokshitzer, V. Khoze, T. Sjostrand, Phys. Lett. **B274**, 116 (1992); J.D. Bjorken, Phys.Rev. **D47**, 101 (1993); R.S. Fletcher, T. Stelzer, ibid. **D48, 5162** (1993).
7. T. Stelzer, Wisconsin PhD thesis (1993).

8. D. Froidevaux, Proc. LHC Workshop, CERN 90-10, Vol.II, p.444.
9. V.Barger, T.Han. R.J.N.Phillips, Phys.Lett.**B206**, 339 (1988).
10. V.Barger et al, Phys.Rev. **D44**, 2701 (1991), **D48**, 5433, 5444(E) (1993).
11. V.Barger, A.D.Martin, R.J.N.Phillips, Phys.Lett. **125B**,339 (1983); V.Barger, T.Han, J. Ohnemus, Phys.Rev. **D37**,1174 (1988).
12. J.M.Cornwall, D.N.Levin, G.Tiktopoulos, Phys.Rev. **D10**,1145(1974); B.W. Lee, C. Quigg, H. Thacker, ibid. **D16**,1519(1977).
13. M.S.Chanowitz, M.K.Gaillard, Nucl.Phys.**B261**, 379 (1985).
14. S.Weinberg, Phys.Rev.Lett.**17**, 11 (1966).
15. J. Bagger et al., Phys. Rev. **D49**, 1246 (1994).
16. S. Nachulich and C.P. Yuan, Phys. Lett. **B293**, 395 (1992).
17. R. Casalbuoni et al, Phys. Lett. **B249**,130; **B253**, 275 (1990).
18. M. Golden in "Beyond the Standard Model" (eds. K. Whisnant, B.L. Young, World Scientific 1989).
19. A. Dobado, M.J. Herrero and J. Terron, Z.Phys.**C50**, 205, 465 (1991).
20. J.Ellis, G.Ridolfi, F.Zwirner, Phys.Lett.**B257**, 83, **B262**, 477 (1991); A. Brignole et al, ibid. **B271**, 123 (1991).
21. V.Barger et al, Phys.Rev. **D45**, 4128, **D46**,4914 (1992).
22. V.Barger, J.L.Hewett, R.J.N.Phillips, Phys.Rev.**D41**, 3421 (1990).
23. J.Hisano, H.Murayama, T.Yanagida, Nucl.Phys.**B402**, 46 (1993).
24. M.Olechowski, S.Pokorski, Phys. Lett. **B214**, 393 (1988).
25. G.Ross, R.G.Roberts, Nucl.Phys. **B377**, 571 (1992).
26. V.Barger, M.S.Berger, P.Ohmann, Phys.Rev. **D47**, 1093 (1993).
27. J.Ellis, G.L.Fogli, E.Lisi, Nucl.Phys. **B393**, 3 (1993).
28. M.A.Diaz, H.E.Haber, Phys.Rev. **D45**, 4246 (1992).
29. G.Isidori, Phys.Lett. **B298**, 409 (1993); J.L.Hewett, ANL-HEP-CP-92-125.
30. J.L.Hewett, Phys.Rev.Lett.**70**,1045(1993); V. Barger, M.S. Berger, R.J.N. Phillips, ibid **70**, 1368 (1993).
31. S.Bertolini et al, Nucl. Phys. **B353**, 591 (1991); R.Barbieri, G.F.Giudice, Phys. Lett. **B309**, 86 (1993).
32. R.M. Godbole, D.P. Roy, Phys. Rev. **D43**, 3641 (1991).
33. J.F. Gunion, Phys. Lett. **B322**, 125 (1994); V. Barger, D.P. Roy, R.J.N. Phillips, ibid **B324**, 236 (1994).
34. H. Baer et al, Phys. Rev. **D47**, 1062 (1993).
35. H.Baer et al, Phys. Rev. **D46**, 1067 (1992).
36. J.F. Gunion et al, Phys. Rev. **D46**, 2040, 2052 (1992); R.M. Barnett et al, ibid **D47**, 1030 (1993).
37. Z. Kunszt, F. Zwirner, Nucl. Phys. **B385**, 3 (1992).
38. V.Barger et al, Phys. Lett. **B314**, 351 (1993).
39. J. Dai, J.F. Gunion, R. Vega, Phys. Lett. **B315**, 355 (1993) and UCD-94-7.
40. V.Barger, K.Cheung, R.J.N.Phillips, A.L.Stange, Phys.Rev. **D47**, 3041 (1993).

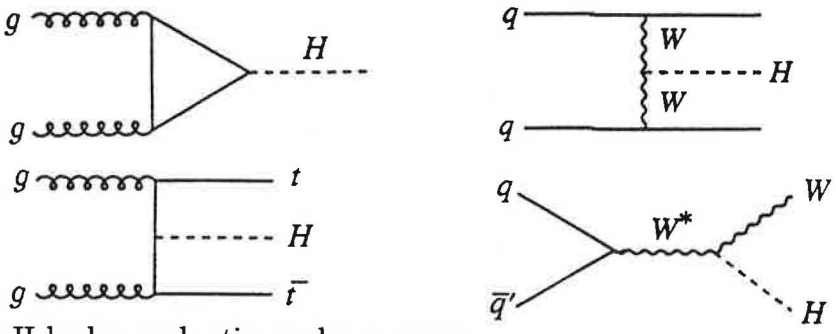

Fig.1. Standard Model H hadroproduction subprocesses.

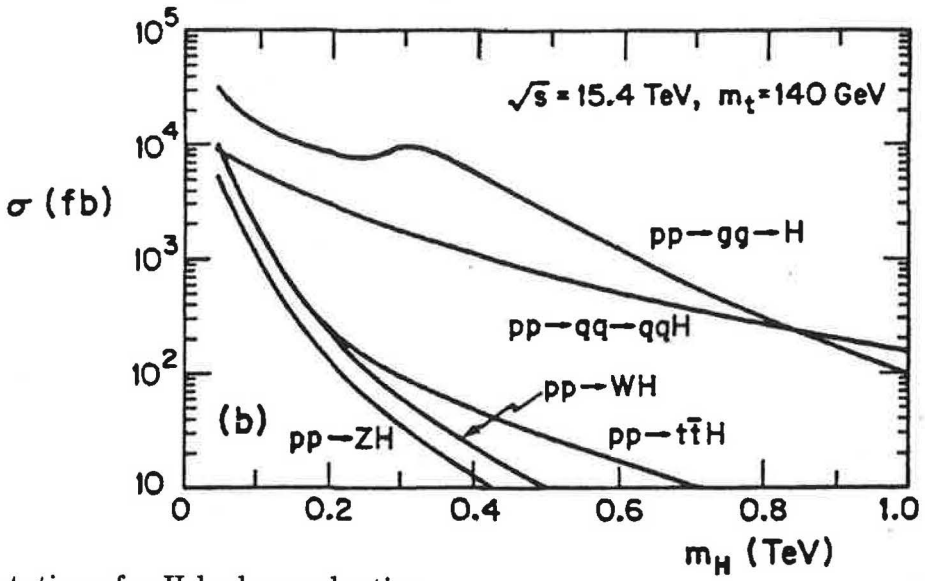

Fig.2. SM expectations for H hadroproduction.

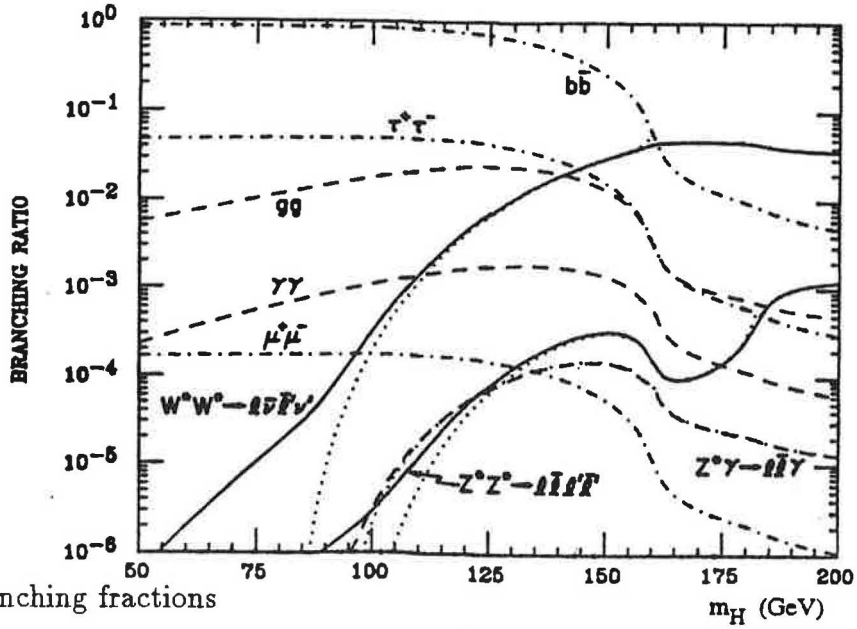

Fig.3. SM Higgs branching fractions

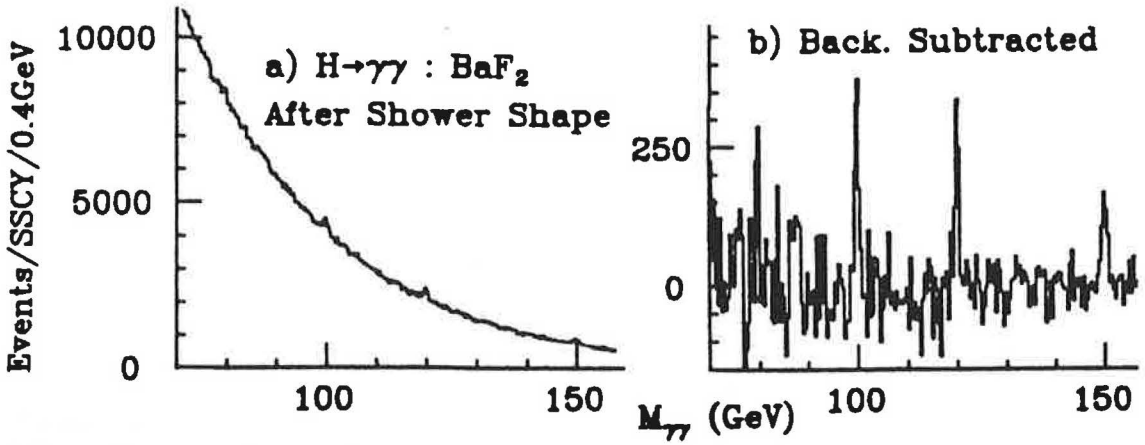

Fig.4. $H \to \gamma\gamma$ signals for m_H = 80, 100, 120, 150 GeV [2].

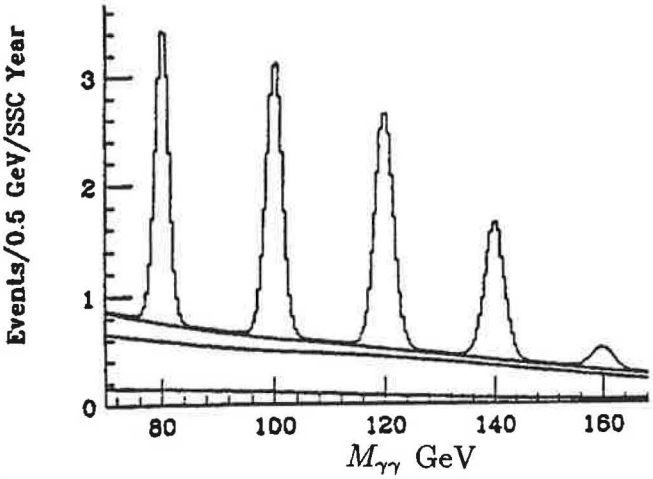

Fig.5. Lepton-tagged $H \to \gamma\gamma$ signals for m_H = 80, 100,..160 GeV [3].

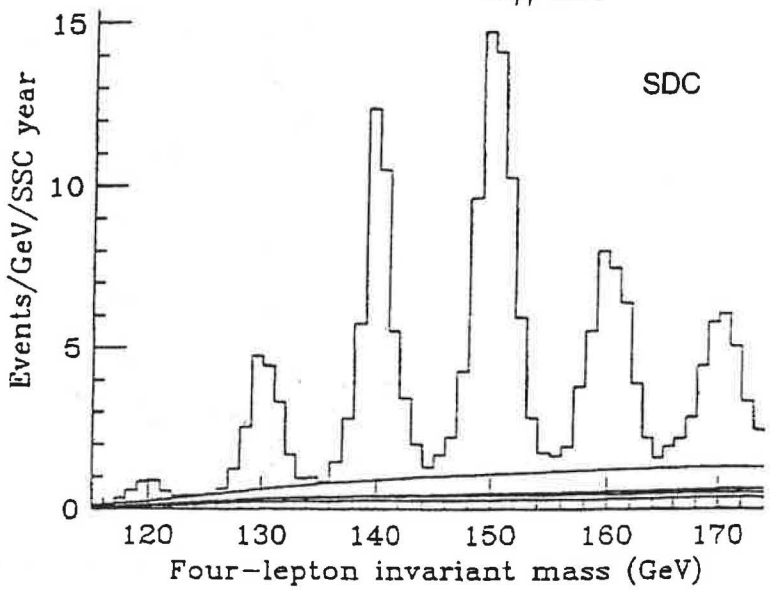

Fig.6. $H \to \ell\bar{\ell}\ell'\bar{\ell}'$ signals for m_H = 120, 130,..170 GeV [3].

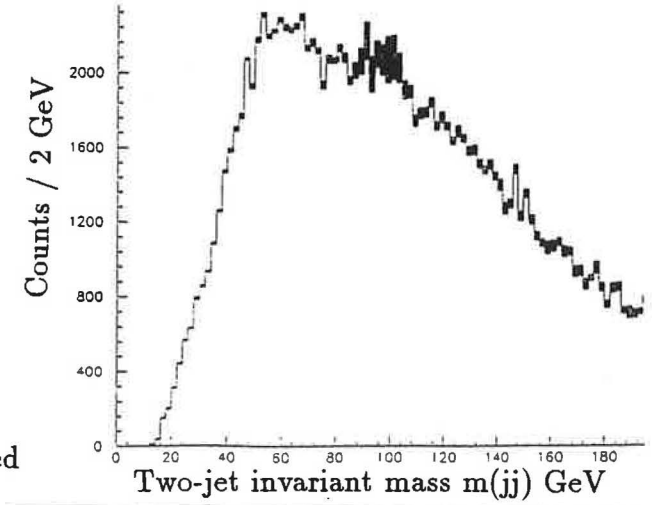

Fig.7. Double-lepton tagged $H \to b\bar{b}$ dijet signal and background for $m_H = 100$ GeV [4]. $t\bar{t}H$ and $t\bar{t}Z$ contributions are shaded

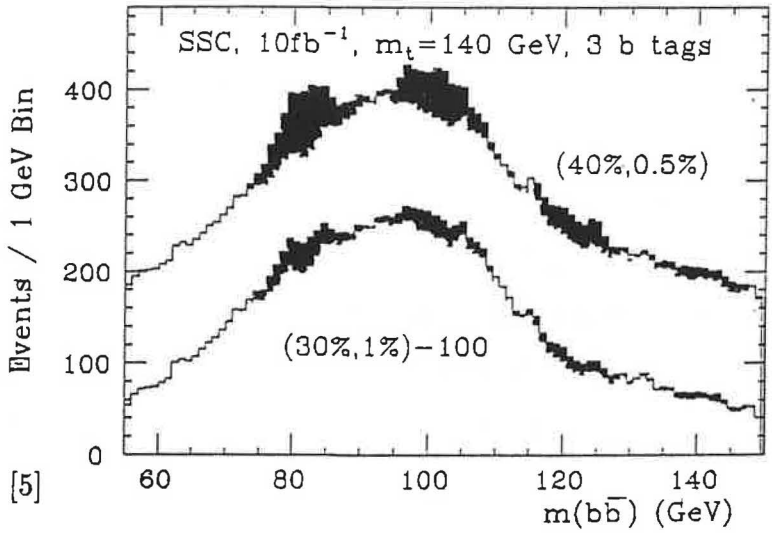

Fig.8. $H \to b\bar{b}$ dijet signals and background with $3-b-jet$ tagging for $m_H = 80, 100, 120, 140 GeV$ [5]

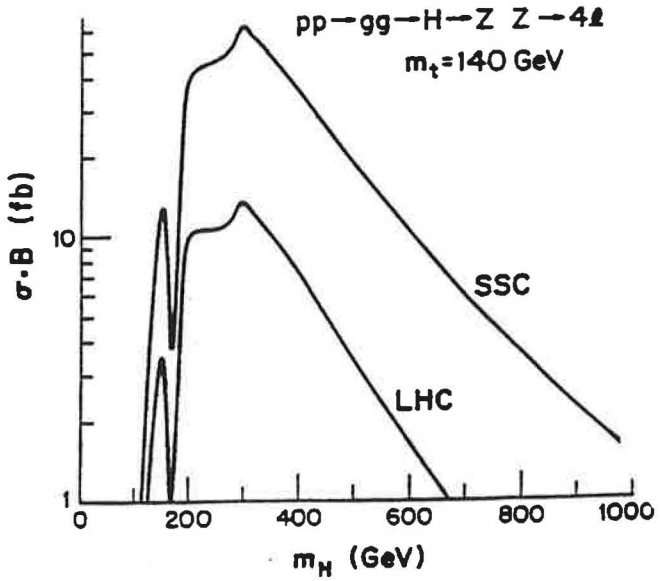

Fig.9 Cross sections for the $H \to \ell\bar{\ell}\ell'\bar{\ell}'$ gold-plated signals at the SSC and LHC .

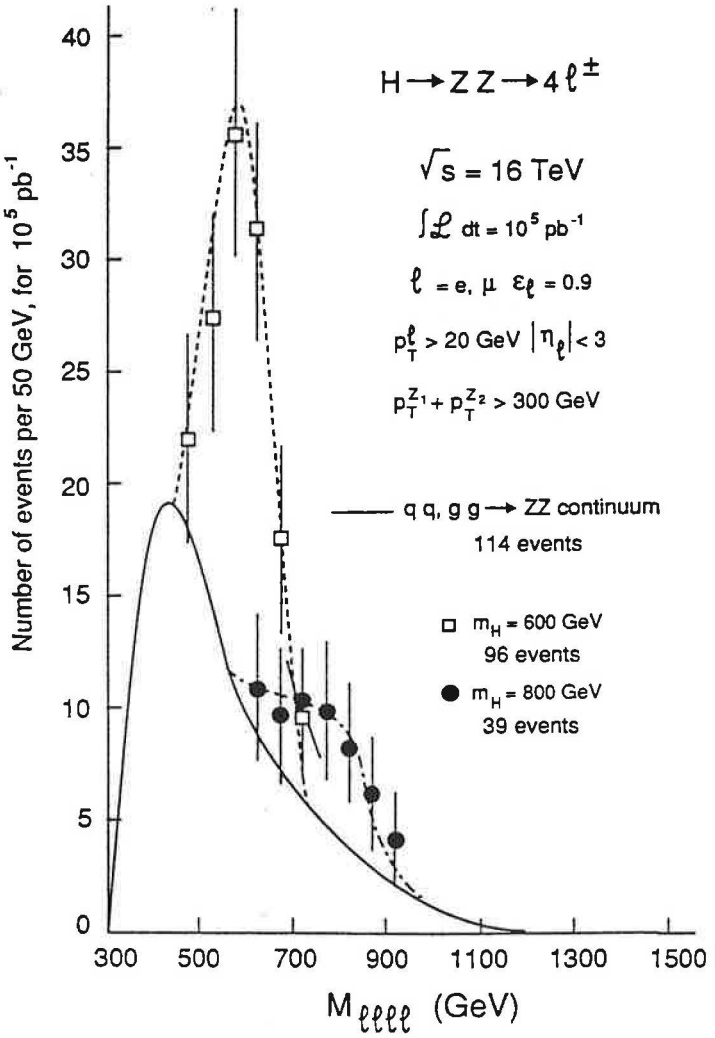

Fig.10
Gold-plated $H \to ZZ \to 4\ell$ mass peaks and background predicted at the CERN LHC for $m_H = 600, 800$ GeV [8]

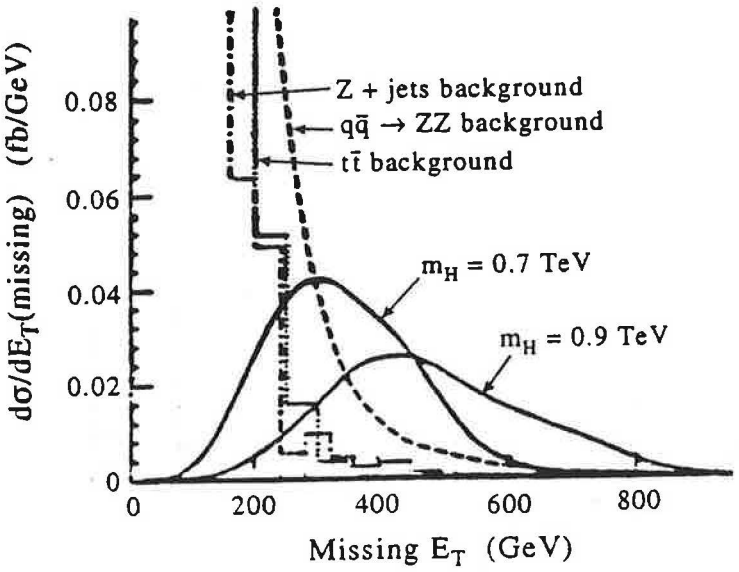

Fig.11.
Silver-plated $H \to ZZ \to \ell\ell\nu\nu$ signals appearing as shoulders in the missing-E_T plot (an SSC example [3]).

Fig.12.
Longitudinal weak
boson scattering
at a pp collider

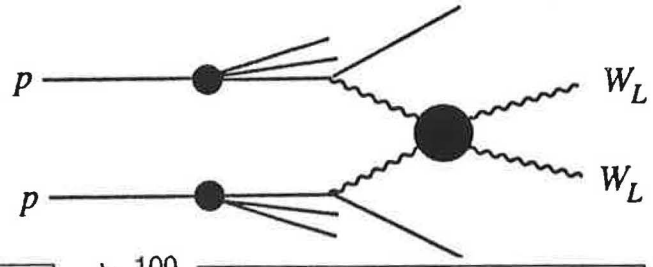

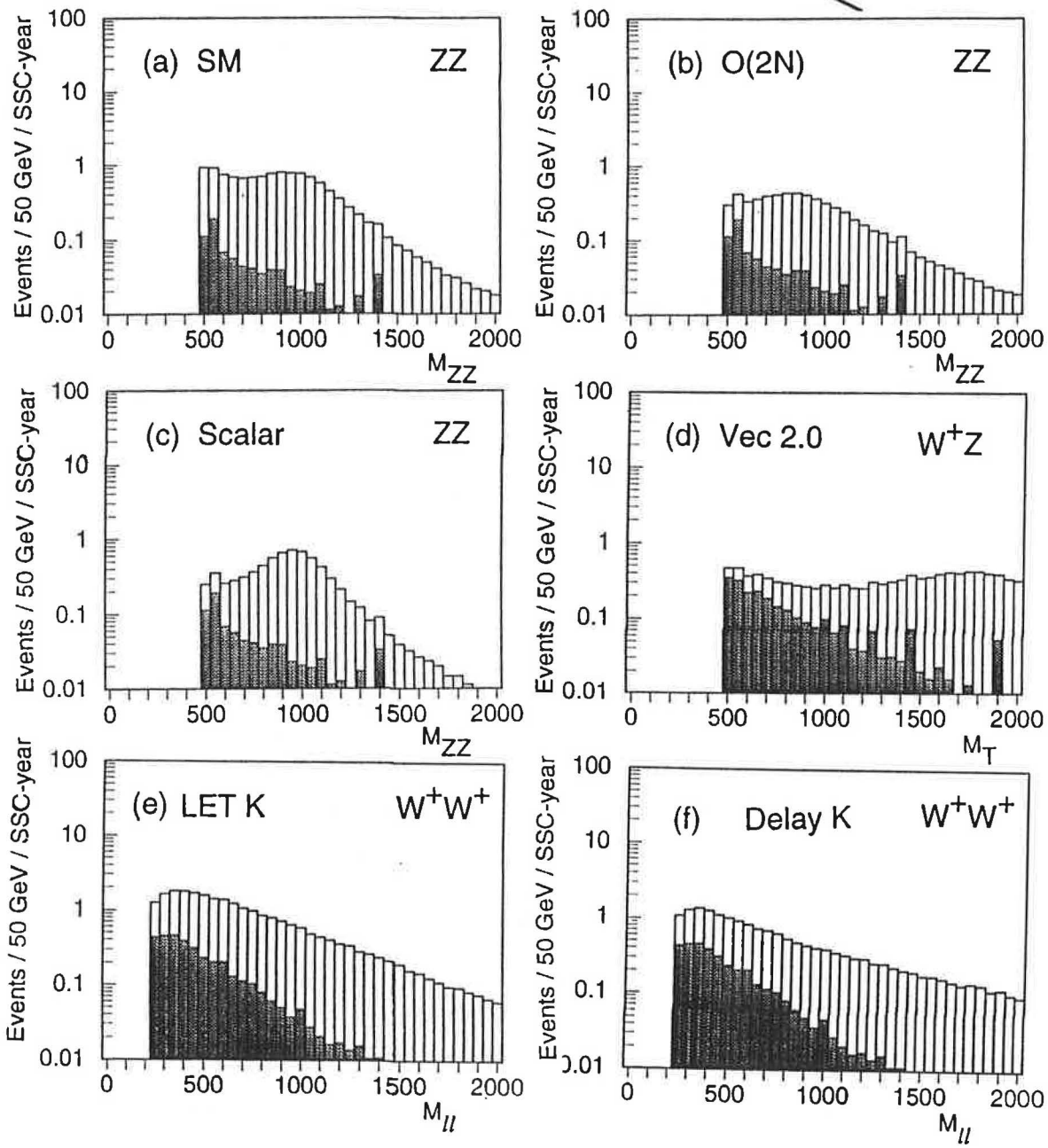

Fig.13. Typical weak-boson scattering signals (unshaded) and backgrounds (shaded)[15].

Fig.14.
Typical t and $\tilde{t}$
one-loop graphs.

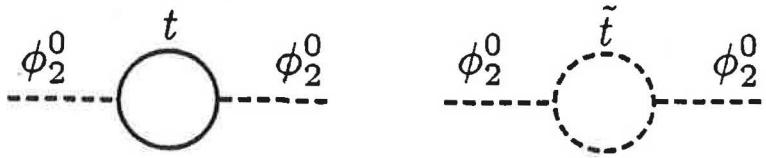

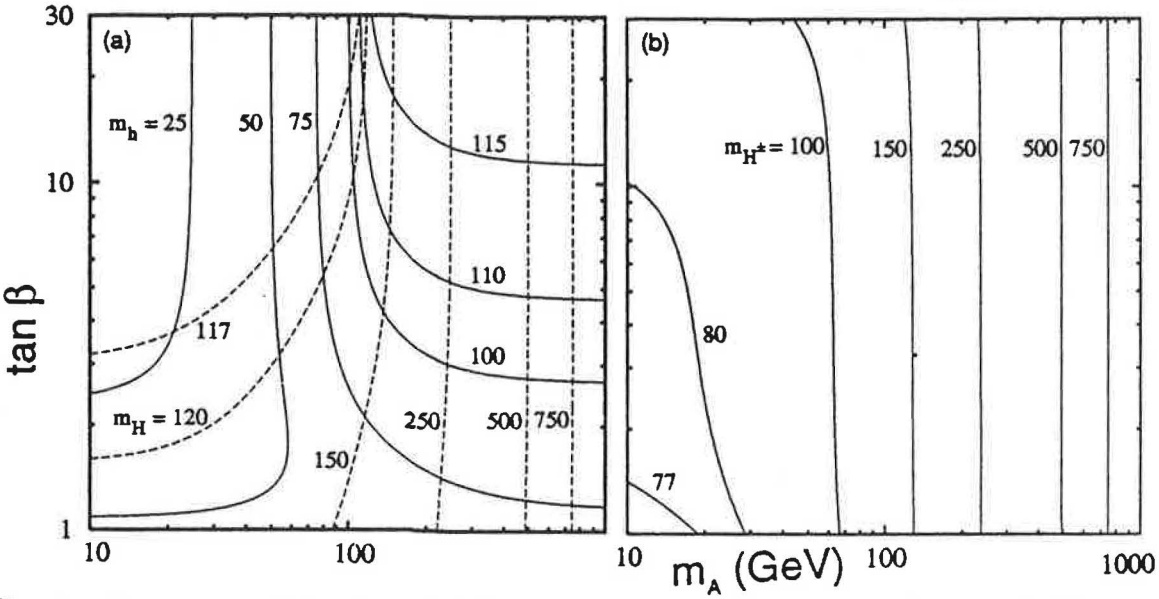

Fig.15. Behaviour of h, H and $H^\pm$ masses in the $(m_A, \tan\beta)$ plane including 1-loop radiative corrections [21].

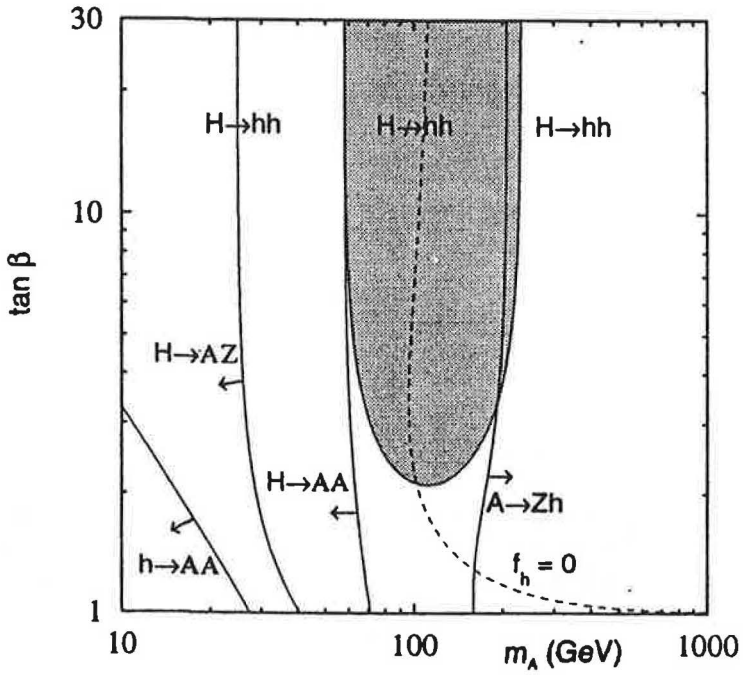

Fig.16. Regions where non-SM neutral Higgs decays compete [21].

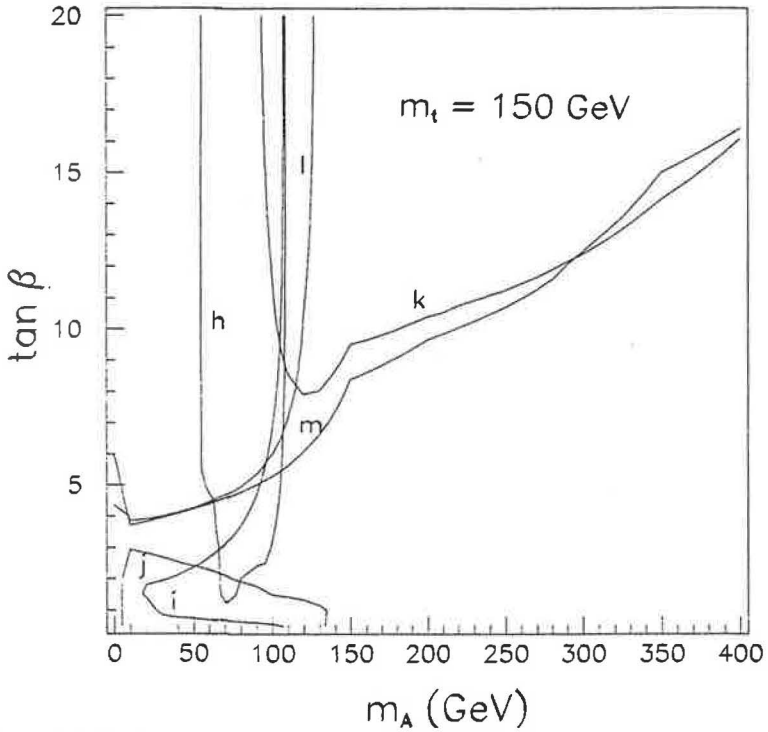

Fig.18. Expected LHC discovery regions for $tth(H,A)$ and $bbh(H,A)$ signals [38].

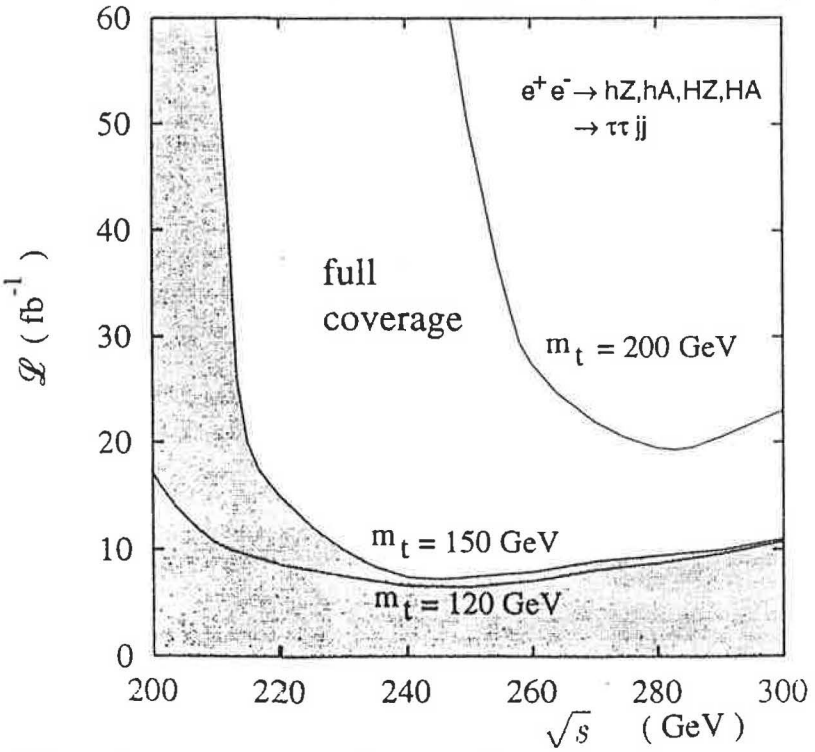

Fig.19. Conditions for covering the $(m_A, \tan\beta)$ parameter space with an e^+e^- collider [39].